Journal of Materials Chemistry A

ROYAL SOCIETY OF CHEMISTRY

PAPER

View Article Online
View Journal | View Issue

Cite this: J. Mater. Chem. A, 2022, 10, 8303

A steric hindrance alleviation strategy to enhance the photo-switching efficiency of azobenzene functionalized metal–organic frameworks toward tailorable carbon dioxide capture†

Qi Huang, [a] Junju Mu,[b] Zhen Zhan,[d] Feng Wang, *[b] Shangbin Jin,*[c] Bien Tan *[d] and Chunfei Wu *[a]

Photo-switching metal–organic frameworks are widely reported for low energy CO_2 capture and release. However, owing to the steric hindrance caused by dense packing of MOF solids, the photo-switching efficiency was still severely restricted. Such an issue then further causes low CO_2 switching capacity and poor regeneration of MOF adsorbents. Herein, we present a strategy to tailor the photo-switching efficiency of azobenzene functionalized MOFs *via* a steric hindrance alleviation approach. An azobenzene-containing Zn based MOF, U-mazo, was designed to decrease the steric hindrance of azo benzene pendants in U-pazo (PCN-123). For comparison, two MOFs without azobenzene, IRMOF-3 and CMOF-2, were also fabricated. Results suggested that compared to U-pazo, the *cis* isomer content in U-mazo increased by 50% upon UV light irradiation at 365 ± 10 nm, which contributed to about 34% enhancement of CO_2 switching efficiency. Density functional theory calculations further explained that the optimized switching efficiency of U-mazo resulted from the lower energy cost for *trans*/*cis* isomerization of azo benzene pendants. Thereby, a promising strategy for optimizing the switching efficiency of the present photoresponsive MOF is explored and verified, and the structural steric hindrance of photoswitching units plays an important role in isomerization of azobenzene-containing MOFs.

Received 28th October 2021
Accepted 1st March 2022

DOI: 10.1039/d1ta09270g

rsc.li/materials-a

Introduction

External stimuli such as light, temperature, pH or magnetic fields can trigger the release of stored substances from host materials, which has been widely researched.[1–3] Among them, light responsive materials have attracted extensive interest owing to their high controllability with instantaneous responsiveness and high accuracy.[4–6] Metal–organic frameworks (MOFs), as 3D crystalline porous organic–inorganic hybrid materials, have been utilized as ideal host materials for CO_2 capture owing to their high porosity and surface area as well as structural tunability and chemical versatility.[7–9] However, the high energy penalty related to MOF adsorbent regeneration through traditional gas liberation technologies strictly limited their large scale application.[10]

Therefore, photo-responsive MOFs have been developed to overcome this challenge by triggering the release of CO_2 under abundant and renewable light.[11–13] Considering the high degree of structural tunability of MOFs, the integration of photochromic units such as azobenzene,[14] diarylethene[15] and spiropyran[16] into MOFs as pendant groups,[17] backbones[18] or guest molecules[19] has been reported to confer photo-switching features to MOFs. Particularly, azobenzene is among the most popular candidates for switching units, not only because of its versatile and simple integration approach,[20] but also owing to its capability of providing alternative CO_2 capture sites.[21] Although many photo-responsive MOFs for low energy CO_2 capture and release have been reported,[22–24] the switching extent and efficiency were still sterically resisted by intermolecular interactions in dense packing of MOF solids.[25] For Instance, Aida *et al.* reported an azobenzene-containing Zr-based ^{Azo}MOF. But only 21% of the ^{Azo}MOF was able to be converted to its *cis* state *via* UV exposure for enough time, which led to a 15% decrease of CO_2 adsorption.[26] Besides, many researchers

[a]School of Chemistry and Chemical Engineering, Queen's University Belfast, Belfast, BT7 1NN, UK. E-mail: c.wu@qub.ac.uk

[b]State Key Laboratory of Catalysis, Dalian National Laboratory for Clean Energy, Dalian Institute of Chemical Physics, Chinese Academy of Sciences, Dalian, 116023, China. E-mail: wangfeng@dicp.ac.cn

[c]School of Chemical Engineering and Technology, Xi'an Jiaotong University, China. E-mail: shangbin@xjtu.edu.cn

[d]School of Chemistry and Chemical Engineering, Huazhong University of Science and Technology, Luoyu Road No. 1037, Wuhan, 430074, China. E-mail: bien.tan@mail.hust.edu.cn

† Electronic supplementary information (ESI) available. See DOI: 10.1039/d1ta09270g

reported that light triggered CO_2 release was still restricted by the switching extent of photochromic units in frameworks.[27–29] Some efforts have been made to enhance the CO_2 switching efficiency, such as introducing CO_2 target active sites, amine, into azo functionalized MOFs[30] or constructing a dual stimuli responsive MOF system with both magnetic and light induction.[31] Nevertheless, these methods cause more complexity of the light responsive system and higher difficulty of preparation, and then increase the cost and energy consumption, which is contrary to the original intention of designing photo-responsive MOFs. Therefore, a new strategy without increasing the cost and complexity of the light responsive system is in significant demand.

Herein, we employed a new strategy to enhance the photo-switching efficiency by tuning the steric hindrance of azo benzene pendants in U-pazo (PCN-123). A series of Zn-based MOFs with and without azobenzene functionalization were fabricated for controllable CO_2 capture. The key to the strategy lies in the tuning of carboxyl acid groups sites on the azo-containing linkers-$^{U\text{-}mazo}$L, which could alleviate the steric hindrance of azobenzene isomerization (Scheme 1). Such a structural tuning strategy was applied to enhance the photo-switching efficiency of U-pazo without increasing the cost and complexity of the light responsive system. The results suggested that integration of azobenzene pendant groups improved the CO_2 capture capacity of U-mazo and U-pazo and endowed them with photo-switching features. Besides, the lower steric hindrance of $^{U\text{-}mazo}$L contributed to the higher switching extent of U-mazo, and finally resulted in a remarkable improvement of CO_2 switching efficiency up to 43% under static conditions. In addition, density functional theory calculation results suggested that ΔE (*trans* to *cis* conversion) of U-mazo was lower than that of U-pazo, which indicated a preferable trend for *trans* to *cis* conversion in U-mazo and further supported the stronger switching ability of U-mazo. The switching property was characterized by UV-visible spectroscopy before and after UV irradiation. The tailorable CO_2 capture performance was demonstrated by adsorption isotherms of CO_2.

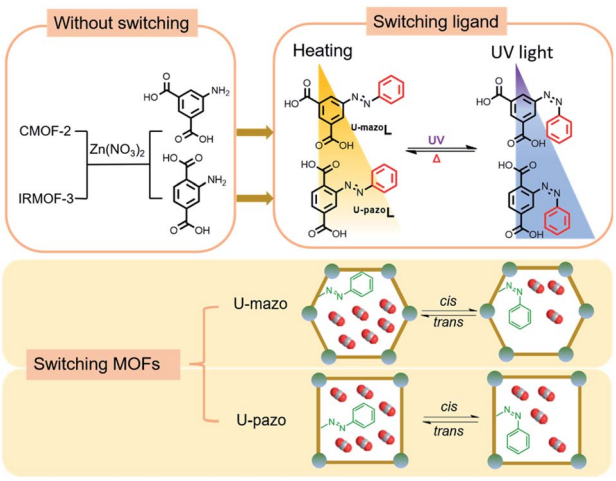

Scheme 1 *Trans*-to-*cis* isomerization of the ligand of U-mazo and U-pazo trigged by UV irradiation and the *cis*-to-*trans* transition triggered by heat treatment.

Experimental section

Materials and methods

Dimethyl 5-aminoisophthalate, nitrosobenzene, dimethyl aminoterephthalate, $Zn(NO_3)_2\cdot 6H_2O$, sodium hydrogen carbonate, anhydrous magnesium sulfate, hydrochloric acid, glacial acetic acid and other common solvents were obtained from commercial suppliers such as Sigma-Aldrich without any further purification.

Fourier-Transformed Infrared (FT-IR) spectra were measured using a Bruker Vertex 70 FTIR spectrometer. The sample was first collected on dried KBr disks, and the spectral range was 500–4000 cm^{-1}. Ultraviolet-visible spectra were obtained by using a UV-VIS-NIR spectrophotometer (UV-3600, Shimadzu Japan) at room temperature. $BaSO_4$ was used as the sample base, and the wavenumber range was set from 200 to 800 cm^{-1}. ^{1}H NMR experiments were performed to check the chemical structure and photo-responsive properties of linkages by using a 400 MHz Bruker with an automated tune and match multi nuclei probe. N_2 and CO_2 adsorption and desorption isotherms were obtained by using a Micromeritics ASAP 2020 M analyzer at 273 K. The temperature was maintained by a bath with refrigeration equipment. Before measurement, the samples were degassed under vacuum conditions (10^{-5} bar) at 80 °C for 8 hours. The CO_2 adsorption heat of U-mazo was calculated from the adsorption isotherm at temperatures of 273 K and 298 K. Thermal stabilities of the samples were measured by Thermogravimetric analysis (TGA) with a PerkinElmer Pyris TGA. The test was performed under conditions of a N_2 atmosphere with a heating rate of 10 °C min^{-1} from room temperature to 800 °C. Powder X-ray diffraction (XRD) was conducted on a Philips X′ Pert Pro. High resolution images of MOF morphologies were measured by using a FEI Sirion 200 field emission scanning electron microscope (FE-SEM).

Synthesis of U-mazo, U-pazo, IRMOF-3 and CMOF-2

A mixture of $Zn(NO_3)_2\cdot 6H_2O$ (1.8 mmol), $^{U\text{-}mazo}$L/5-aminoisophthalic acid (0.6 mmol) and 50 mL DMA was sealed in a 100 mL Teflon-lined autoclave. At the same time, $Zn(NO_3)_2\cdot 6H_2O$ (1.8 mmol), $^{U\text{-}pazo}$L/2-aminoterephthalic acid (0.6 mmol) and DMF (50 mL) were sealed in a 100 mL Teflon-lined autoclave. The two reaction systems were heated at 85 °C for 3 days at the same time. After cooling down the reaction system, the four product crystals were collected by filtration, and then washed with DMF and CH_2Cl_2 to get the final products U-mazo, CMOF-2, U-pazo and IRMOF-3, respectively.

Characterization of photoisomerization in linkages and MOFs

Measurement of the *cis* isomer content in $^{U\text{-}mazo}$L and $^{U\text{-}pazo}$L: the samples were dissolved with DMSO-d_6 in NMR tubes and then irradiated with UV LED strips (360 nm ± 10 nm) followed by heating with different time segments. The sampling tubes

were shortly tested for the ^{1}H NMR spectra to determine the *cis* isomer content. As shown in Fig. 2a and b, the signal at δ7.4 is assigned to the *trans* isomer of $^{U\text{-}pazo}$L while those new blue peaks at δ6.8 correspond to the *cis* isomer. As for $^{U\text{-}mazo}$L, the *trans* isomer signal was at δ8.6 while the *cis* isomer signal was at δ8.1. Therefore, the *cis* isomer content was defined as $I_{cis}/(I_{trans} + I_{cis})$.

CO_2 switching adsorption and desorption cycles: the original sample was first degassed under vacuum conditions (10^{-5} bar) at 80 °C for 8 hours and the CO_2 adsorption and desorption isotherm test was carried out by using a Micromeritics ASAP 2020 M analyzer. After this test, the sample was sandwiched as a thin film between two quartz glass plates and then was uniformly irradiated with UV light from both directions. After 5 hour UV light irradiation, the sample was collected for the further ASAP CO_2 adsorption and desorption test without the heating procedure. After finishing the test, the sample was degassed with heating for 8 hours again and then evaluated again by ASAP for the reversibility test. Such a process was repeated for three cycles for CO_2 switching isomerization cycles of U-mazo.

Photoisomerization cycles of UV-Vis absorption spectra: $BaSO_4$ was used as a reference sample. First, the sample was added on the surface of $BaSO_4$ and tested for UV-Vis absorption spectra. The sample plate was then irradiated with UV light for 5 hours and then directly tested *via* UV-Vis spectroscopy again for characterization of *trans* to *cis* switching. After the UV-Vis spectroscopy test, the sample plate was then transferred to a vacuum oven for heating at 80 °C. After heating, the sample plate was tested *via* UV-Vis spectroscopy again for characterization of *cis* to *trans* back switching. Such a process was then repeated for five cycles for photoisomerization cycles of U-mazo.

Results and discussion

In this work, two azobenzene functionalized MOFs, U-mazo and U-pazo, were synthesized by a hydrothermal method, and CMOF-2 and IRMOF-3 were fabricated as the control samples without azobenzene. Compared to IRMOF-3 and CMOF-2, the obvious red-orange colour of U-mazo and U-pazo directly indicated the presence of azobenzene pendants in the frameworks (Fig. S2 in the ESI†). Besides, the incorporation of azobenzene bonding in U-mazo and U-pazo was further supported *via* the FTIR spectra (Fig. S3a in the ESI†) where the characteristic peaks at 1444 cm^{-1} corresponded to the N=N bonding of azo groups. For CMOF-2, the peaks centered at 1430, 1530 and 1610 cm^{-1} were attributed to the C=C of azo phenyl groups. In addition, the two sharp bands around 1572 and 1362 cm^{-1} are attributed to the asymmetric (υ_s(C–O)) and symmetric (υ_s(C–O)) vibrations of carboxyl groups, respectively. Powder X-ray diffraction patterns (Fig. 1) were applied to estimate the crystal structure of the MOFs. Since the azobenzene group was relatively bulky, the integration of the groups could impact the crystallization process and then led to the different crystalline structures of U-mazo and CMOF-2. For the same reason, U-pazo and IRMOF-3 also suggested different crystalline structures. However, all peaks of U-mazo and U-pazo were completely

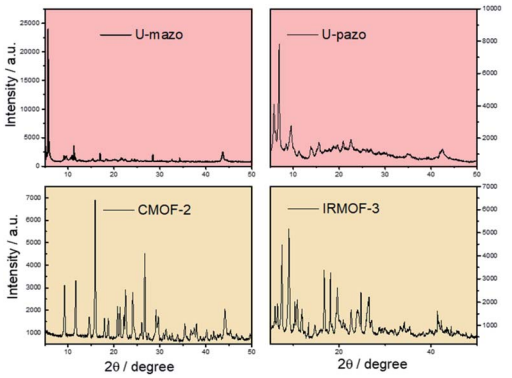

Fig. 1 Powder X-ray diffraction patterns of MOFs.

consistent with reported PCN-123 (ref. 32) and JUC-128 (ref. 33) patterns that were synthesized using the same linkers and metals. It is demonstrated that the correct structure of U-mazo and U-pazo was developed.

Scanning electron microscopy (Fig. S4 in the ESI†) was employed to image the MOF samples. Both IRMOF-3 and U-pazo showed cubic crystals with particle sizes relatively larger than IRMOF-3. In addition, U-mazo and CMOF-2 indicated similar rod shapes. Therefore, the particle shape of either U-mazo or U-pazo was not influenced by the incorporation of azobenzene. To further investigate the elemental distribution of U-mazo and U-pazo, SEM mapping was also performed (Fig. S5 in the ESI†). Both U-mazo and U-pazo indicated uniform distribution of N, O, and Zn. Thermogravimetric (TGA) analysis was conducted to characterize the thermal stability of the MOF samples. As shown in Fig. S6,† each sample showed two steps of mass loss in TGA curves. The first and second stages of mass loss of these samples could be attributed to the dissolution of MOF frameworks and decomposition of linkages, respectively. The first mass loss of U-mazo and U-pazo starts at 200 and 170 °C, respectively, indicating lower thermal stability than CMOF-2 and IRMOF-3. Therefore, the incorporation of azobenzene pendants caused lower thermal stability of MOF frameworks of U-mazo and U-pazo. In addition, the second mass loss stage of U-mazo and U-pazo also occurred earlier than CMOF-2 and IRMOF-3, which was ascribed to the easier decomposition of azo groups of ligands under high temperature.

Photoswitching properties of linkages of U-mazo and U-pazo were characterized and compared using ^{1}H NMR spectra in DMSO-d_6 (Fig. 2a and b). Both original $^{U\text{-}mazo}$L and $^{U\text{-}pazo}$L (black coloured spectrum) were converted to the *cis* isomer (blue coloured spectrum) upon irradiation with UV light (360 ± 10 nm), and then underwent isomerization back to the *trans* form (red coloured spectrum) *via* simple heating. It is suggested that the isomerization process is reversible. However, as shown in Fig. S7 in the ESI,† the switching rate and extent of the two linkages were different. The *trans* to *cis* transition of $^{U\text{-}mazo}$L upon UV exposure was established in 1 hour with a *cis* isomer content of 53%, while only 37% *cis* isomer was obtained for $^{U\text{-}pazo}$L at the same time. Such results demonstrated the higher

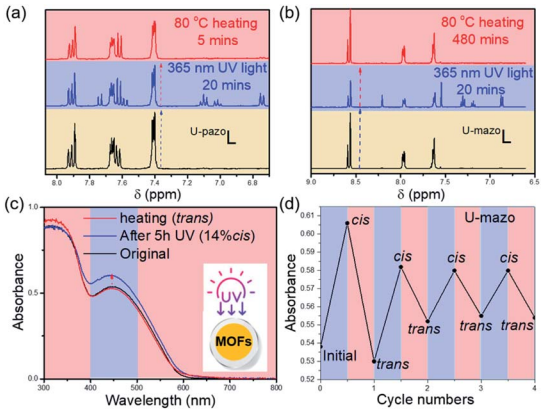

Fig. 2 ^{1}H NMR spectra of a fresh ligand (a) $^{U\text{-}pazo}$L and (b) $^{U\text{-}mazo}$L solution (DMSO-d_6) after 365 ± 10 nm irradiation for 20 min, heating (a) $^{U\text{-}pazo}$L for 5 min and heating (b) $^{U\text{-}mazo}$L for 480 min at 80 °C. (c) Solid UV-Vis spectra of U-mazo at 25 °C in the solid state upon irradiation with UV (365 ± 10 nm) and then heating at 80 °C. (d) Repetitive photoisomerization cycles of U-mazo. The same isomerization was repeated for three more cycles.

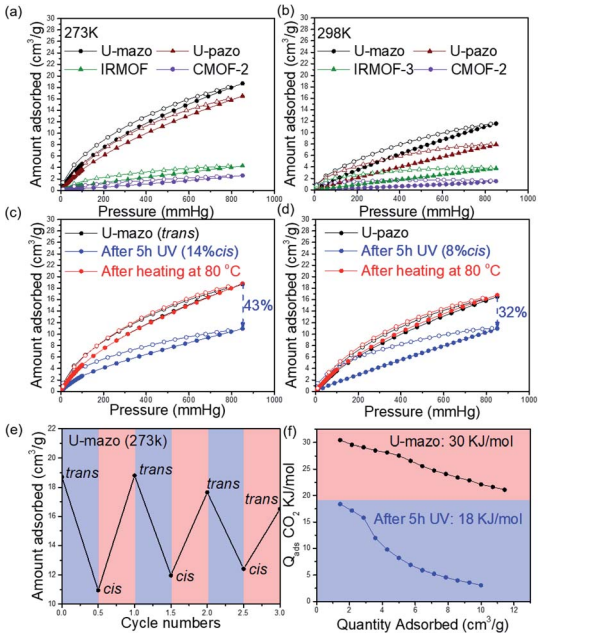

Fig. 3 CO_2 adsorption and desorption isotherms (a) at 273 K and (b) 298 K of MOFs. CO_2 adsorption isotherms (at 273 K) of (c) U-mazo and (d) U-pazo showing conformational changes: right after the first UV irradiation at 365 ± 10 nm (blue) and heating at 80 °C. (e) Adsorption cycles of U-mazo for CO_2 upon *trans* and *cis* photoisomerization; (f) CO_2 heat of adsorption of U-mazo and after 5 hour UV irradiation (365 ± 10 nm).

switching efficiency of $^{U\text{-}mazo}$L, which was attributed to the lower steric hindrance of azobenzene in $^{U\text{-}mazo}$L. Therefore, such a steric hindrance alleviation strategy by tuning carboxyl acid groups sites can successfully enhance the photoswitching efficiency of $^{U\text{-}pazo}$L. However, after the coordination reaction, the switching condition in the solid state of frameworks could be totally different with free molecules dissolved in solution. The photo-switching efficiency of U-mazo and U-pazo as MOF solids also needs to be further investigated and compared.

The switching properties of U-mazo (Fig. 2c) and U-pazo (Fig. S8 in the ESI†) were also characterized and compared *via* UV/Vis spectroscopy. Under UV light irradiation, both U-mazo and U-pazo showed an enhancement of the n–π* transition band between 400 and 500 nm, corresponding to the occurrence of the *trans* to *cis* transition of azobenzene pendants in the frameworks. Through subsequent heating at 80 °C, the azobenzene pendants were converted back to *trans* isomers, indicating a reversible isomerization process of U-mazo and U-pazo, respectively. More importantly, a higher switching content of U-mazo was also observed in the UV/Vis spectra, which was consistent with the results of linkages. In detail, the photostationary state of U-mazo upon UV exposure was established at 14% *cis* isomer while U-pazo only achieved 8% *cis* isomer under the same conditions. Apart from that, such forward and backward photo-isomerization processes could be recycled three times with a slight decrease in second repeats and swiftly achieve stability for the subsequent cycles. These results further support that the lower steric hindrance of azobenzene side groups can greatly contribute to an optimized photo-switching efficiency of both $^{U\text{-}mazo}$L and U-mazo.

The CO_2 uptake ability of U-mazo and CMOF-2 was first investigated here at 273 K and 298 K. In addition, U-pazo and IRMOF-3 were also compared under the same conditions to explore the influence of the introduction of azobenzene groups on CO_2 capture performance. As shown in Fig. 3a, the CO_2 uptake capacity of U-mazo was far higher than that of its non-azo benzene functionalized CMOF-2, increasing around 7 times at 273 K and 1 bar. The same trend can also be observed for U-pazo and CMOF-2: azo benzene-containing U-pazo demonstrated around 4 times higher CO_2 uptake capacity than IRMOF-3. These results suggested an enhanced CO_2 adsorption performance of the MOF frameworks in the presence of azobenzene pendants, which was consistent with previous investigations.[21]

Notably, compared to previously reported U-pazo (PCN-123), U-mazo developed in this work exhibited an optimized dynamic photo-switching CO_2 adsorption behavior upon *trans*/*cis* isomerization. After 5 hours of 360 nm UV light irradiation, the CO_2 uptake capacity of U-mazo decreased from 0.83 to 0.49 mmol g^{-1} upon *trans* to *cis* isomerization, indicating an up to 43% decrease in CO_2 uptake (Fig. 3c). In addition, such adsorption capacity could be recovered to its original state by simple heating at 80 °C, corresponding to a reversible CO_2 switching process. However, U-pazo only showed a 32% decline of CO_2 adsorption capacity upon UV exposure (Fig. 3d), reflecting an optimized CO_2 switching efficiency of U-mazo. Such superior CO_2 switching performance of U-mazo was comparable to those of many reported photo-responsive materials (Table S2 in the ESI†). Apart from that, the CO_2 adsorption isotherm of CMOF-2 and IRMOF-3 under UV irradiation was also determined for controlled experiments (Fig. S9 in the ESI†). The results suggested that CO_2 capture ability was still similar even under 5 hour UV irradiation, which demonstrated that the CO_2

switching performance of U-mazo and U-pazo resulted from the incorporation of photochromic units. Therefore, azobenzene functionalization in U-mazo and U-pazo not only leads to a higher CO_2 adsorption capacity but also endows them with tailorable CO_2 capture ability. Moreover, the lower steric hindrance of azobenzene pendants in U-mazo led to faster and superior photoisomerization properties and then contributed to the enhanced CO_2 switching efficiency of U-mazo.

ΔE values upon *trans*/*cis* isomerization of U-mazo and U-pazo were calculated by using the density functional theory method to support the experimental results. The $\Delta E_{(trans\ \text{to}\ cis)}$ of U-mazo and U-pazo was calculated to be 47.2 and 54.2 kJ mol^{-1}, respectively. The lower $\Delta E_{(trans\ \text{to}\ cis)}$ of U-mazo confirmed the relatively easier *trans* to *cis* transition of azobenzene units in U-mazo, which further supported the greater switching extent and enhanced CO_2 switching efficiency of U-mazo.

Regeneration of U-mazo was also studied as shown in Fig. 3e. The CO_2 switching process upon *trans*/*cis* isomerization was performed three times, with a slight decrease of switching efficiency, indicating the reversibility and stability of the present adsorbents upon continuous UV exposure. In addition, the FTIR spectrum (Fig. S10 in the ESI†) showed minor changes even after 15 hours of UV irradiation, further confirming the structural stability of U-mazo. Since CO_2 heat adsorption (Q_{ads}) is related to the interaction strength between CO_2 molecules and MOF adsorbents, the Q_{ads} of U-mazo under its UV irradiated and non-irradiated state was also estimated to explore the mechanism for light induced CO_2 switching behavior. As shown in Fig. 3f, the original Q_{ads} of U-mazo was around 31 kJ mol^{-1} in the *trans* isomer state, but the value decreased to 17 kJ mol^{-1} under UV light irradiation. Thus, the CO_2 molecule showed weaker affinity toward the U-mazo framework in the UV irradiated *cis* state than its non-irradiated *trans* state. This explains the dramatic decrease of CO_2 uptake capacity upon UV exposure, achieving a tailorable CO_2 capture approach with low energy.[34]

N_2 adsorption isotherms of all MOF samples were used for characterizing the CO_2/N_2 selectivity. Surprisingly, a clear decrease of N_2 adsorption capacity of both U-mazo and U-pazo was observed upon the *trans* to *cis* isomerization of azobenzene units. These results further confirmed that steric hindrance played an important role in causing the CO_2 adsorption capacity swings of U-mazo and U-pazo. In addition, the adsorption isotherms of U-mazo and U-pazo showed relatively low capacities for N_2 adsorption (Fig. 4), indicating preferable binding with CO_2 molecules and high selectivity for CO_2 over N_2. Compared to CMOF-2 and IRMOF-3 (Fig. S11 in the ESI†), the CO_2/N_2 selectivity of U-mazo and U-pazo was dramatically improved, indicating another advantage of the incorporation of azobenzene units. Apart from high CO_2/N_2 selectivity, a light induced selectivity swing was also observed. Henry's constants were used to estimate the CO_2/N_2 selectivity of U-mazo and U-pazo. It is suggested that U-mazo has a CO_2/N_2 selectivity of 334 in the *trans* state and 226 in the *cis* state at 273 K, indicating a light induced CO_2/N_2 selectivity swing. Interestingly, after 5 hour UV irradiation, U-pazo showed an increase of CO_2/N_2 selectivity from 100 to 148 at 273 K. Therefore, CO_2/N_2 selectivity could also be adjusted by remote light control during gas separation.

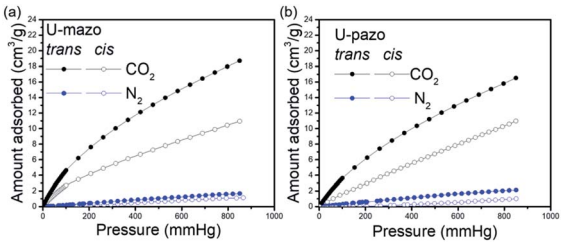

Fig. 4 CO_2 and N_2 adsorption isotherms of (a) U-mazo and (b) U-pazo at 273 K and the isotherms right after the first UV irradiation at 365 ± 10 nm (blue).

As the performance of CO_2 and N_2 uptake is largely connected to pore properties, the BET surface area and pore size distributions of U-mazo and U-pazo in *cis* and *trans* isomer states were determined *via* N_2 adsorption isotherms obtained at 77 K. As shown in Table S11 and Fig. S12,† both U-mazo and U-pazo indicated a relatively low BET surface area. The obtained CO_2 uptakes could come from the restricted pores in which it is hard for N_2 molecules to enter. However, the influence of isomerization on porosity changes can still be observed. Both U-pazo and U-mazo suggested a decrease of BET surface area and pore volume upon *trans* to *cis* isomerization, which then could lead to the decrease of CO_2 and N_2 uptake capacities. Apart from that, the pore size distribution of U-mazo and U-pazo also changed after the UV light irradiation. As shown in Fig. S13,† pristine U-mazo contained a small content of micropores. After the UV light irradiation, the micropore volume obviously decreased, which resulted from the light-induced isomerization of azo ligands. In addition, the UV light irradiation of U-pazo led to a decrease of micropore volume, which then could contribute to the decline of CO_2 and N_2 uptake capacities. These results demonstrate that photoisomerization of ligands in U-mazo and U-pazo could lead to pore size distribution changes, and then contribute to tailorable CO_2 and N_2 capture.

Conclusion

In summary, a series of Zn-based MOFs were fabricated, including U-mazo and U-pazo, which were functionalized with azobenzene groups to effectively tailor the CO_2 capture properties. Experimental results indicated that the incorporation of azobenzene pendants not only enhanced their capacity and selectivity of CO_2 adsorption but also endowed them with tailorable CO_2 capture ability. More importantly, the lower steric hindrance of photochromic units in U-mazo contributed to enhanced higher CO_2 switching efficiency, which was supported by the DFT calculation analysis. In addition, both U-mazo and U-pazo exhibited a high adsorption selectivity for CO_2 over N_2, and such selectivity could be switched upon *trans*/*cis* isomerization. Therefore, the enhanced tailorable CO_2 capture combined with high selectivity *via* a structural strategy gives them more potential for gas separation in a realistic application. A promising strategy is then successfully developed to

improve the CO_2 switching efficiency of photoresponsive MOFs, promoting practical applications of using photo-switching MOFs for CO_2 capture.

Conflicts of interest

There are no conflicts to declare.

Acknowledgements

The authors sincerely appreciate the financial support from the China Scholarship Council. This project has received funding from the European Union's Horizon 2020 research and innovation program under the Marie Skłodowska–Curie grant agreement no. 823745.

Notes and references

1 J. Ge, E. Neofytou, T. J. Cahill, III, R. E. Beygui and R. N. Zare, *ACS Nano*, 2012, **6**, 227–233.
2 R. P. Johnson, Y. Jeong, E. Choi, C. Chung, D. H. Kang, S. Oh, H. Suh and I. Kim, *Adv. Funct. Mater.*, 2012, **22**, 1058–1068.
3 M. Ishaq, M. A. Gilani, I. Arshad, M. R. Bilad, F. Ahmad and A. L. Khan, *Carbon Capture Sci. Technol.*, 2021, **1**, 100019.
4 A. Modrow, D. Zargarani, R. Herges and N. Stock, *Dalton Trans.*, 2011, **40**, 4217–4222.
5 R. Haldar, L. Heinke and C. Woll, *Adv. Mater.*, 2019, e1905227.
6 S. Garg, H. Schwartz, M. Kozlowska, A. B. Kanj, K. Müller, W. Wenzel, U. Ruschewitz and L. Heinke, *Angew. Chem., Int. Ed.*, 2019, **58**, 1193–1197.
7 R. Lyndon, K. Konstas, B. P. Ladewig, P. D. Southon, P. C. Kepert and M. R. Hill, *Angew. Chem., Int. Ed.*, 2013, **52**, 3695–3698.
8 H. Demir, G. O. Aksu, H. C. Gulbalkan and S. Keskin, *Carbon Capture Sci. Technol.*, 2022, **2**, 100026.
9 L. Gong Le, X. F. Feng and F. Luo, *Inorg. Chem.*, 2015, **54**, 11587–11589.
10 A. B. Kanj, K. Müller and L. Heinke, *Macromol. Rapid Commun.*, 2018, **39**, 1700239.
11 D. Hermann, H. A. Schwartz, M. Werker, D. Schaniel and U. Ruschewitz, *Chemistry*, 2019, **25**, 3606–3616.
12 H. Agarkar and D. Das, *J. Mol. Struct.*, 2019, **1184**, 435–442.
13 C. T. Yang, A. R. Kshirsagar, A. C. Eddin, L. C. Lin and R. Poloni, *Chemistry*, 2018, **24**, 15167–15172.
14 J. W. Brown, B. L. Henderson, M. D. Kiesz, A. C. Whalley, W. Morris, S. Grunder, H. Deng, H. Furukawa, J. I. Zink, J. F. Stoddart and O. M. Yaghi, *Chem. Sci.*, 2013, **4**, 2858–2864.
15 I. M. Walton, J. M. Cox, J. A. Coppin, C. M. Linderman, D. G. Patel and J. B. Benedict, *Chem. Commun.*, 2013, **49**, 8012–8014.
16 U. G. Randika Lakmali and C. V. Hettiarachchi, *CrystEngComm*, 2015, **17**, 8607–8611.
17 R. Huang, M. R. Hill, R. Babarao and N. V. Medhekar, *J. Phys. Chem. C*, 2016, **120**, 16658–16667.
18 D. G. Patel, I. M. Walton, J. M. Cox, C. J. Gleason, D. R. Butzer and J. B. Benedict, *Chem. Commun.*, 2014, **50**, 2653–2656.
19 D. Hermann, H. Emerich, R. Lepski, D. Schaniel and U. Ruschewitz, *Inorg. Chem.*, 2013, **52**, 2744–2749.
20 K. Müller, J. Wadhwa, J. Singh Malhi, L. Schottner, A. Welle, H. Schwartz, D. Hermann, U. Ruschewitz and L. Heinke, *Chem. Commun.*, 2017, **53**, 8070–8073.
21 Y. Qiao, Z. Zhan, Y. Yang, M. Liu, Q. Huang, B. Tan, X. Ke and C. Wu, *Mater. Today Commun.*, 2021, **27**, 102338.
22 R. Lyndon, K. Konstas, A. W. Thornton, A. J. Seeber, B. P. Ladewig and M. R. Hill, *Chem. Mater.*, 2015, **27**, 7882–7888.
23 W. An, D. Aulakh, X. Zhang, W. Verdegaal, K. R. Dunbar and M. Wriedt, *Chem. Mater.*, 2016, **28**, 7825–7832.
24 S. Castellanos, A. Goulet-Hanssens, F. Zhao, A. Dikhtiarenko, A. Pustovarenko, S. Hecht, J. Gascon, F. Kapteijn and D. Bleger, *Chem.–Eur. J.*, 2016, **22**, 746–752.
25 F. Bigdeli, C. T. Lollar, A. Morsali and H. C. Zhou, *Angew. Chem., Int. Ed.*, 2020, **59**, 4652–4669.
26 H. Huang, H. Sato and T. Aida, *J. Am. Chem. Soc.*, 2017, **139**, 8784–8787.
27 H. Li, M. R. Martinez, Z. Perry, H. C. Zhou, P. Falcaro, C. Doblin, S. Lim, A. J. Hill, B. Halstead and M. R. Hill, *Chem.–Eur. J.*, 2016, **22**, 11176–11179.
28 W. C. Song, X. Z. Cui, Z. Y. Liu, E. C. Yang and X. J. Zhao, *Sci. Rep.*, 2016, **6**, 34870.
29 N. Prasetya and B. P. Ladewig, *Sci. Rep.*, 2017, **7**, 13355.
30 Y. Jiang, P. Tan, S. C. Qi, X. Q. Liu, J. H. Yan, F. Fan and L. B. Sun, *Angew. Chem., Int. Ed.*, 2019, **58**, 6600–6604.
31 H. Li, M. M. Sadiq, K. Suzuki, C. Doblin, S. Lim, P. Falcaro, A. J. Hill and M. R. Hill, *J. Mater. Chem. A*, 2016, **4**, 18757–18762.
32 J. Park, D. Yuan, K. T. Pham, J. Li, A. Yakovenko and H. Zhou, *J. Am. Chem. Soc.*, 2012, **134**, 99–102.
33 H. He, J. Du, H. Su, Y. Yuan, Y. Song and F. Sun, *CrystEngComm*, 2015, **17**, 1201–1209.
34 N. Prasetya, B. C. Donose and B. P. Ladewig, *J. Mater. Chem. A*, 2018, **6**, 16390–16402.